Cleaner Engineering and Technology 9 (2022) 100538

Contents lists available at ScienceDirect

Cleaner Engineering and Technology

journal homepage: www.sciencedirect.com/journal/cleaner-engineering-and-technology

Catalytic Co-pyrolysis of empty fruit bunch and high-density polyethylene mixtures over rice husk ash: Thermogravimetric, kinetic and thermodynamic analyses

Nadhilah Aqilah Shahdan [a], Vekes Balasundram [a,*], Norazana Ibrahim [b], Ruzinah Isha [c], Zainuddin Abdul Manan [d]

[a] Malaysia-Japan International Institute of Technology, Universiti Teknologi Malaysia, 54100, Kuala Lumpur, Malaysia
[b] Energy Research Group, School of Chemical and Energy Engineering, Faculty of Engineering, Universiti Teknologi Malaysia, 81310, Johor Bahru, Johor, Malaysia
[c] College of Engineering, Universiti Malaysia Pahang, 26600, Pekan, Pahang, Malaysia
[d] Process Systems Engineering Centre (PROSPECTS), School of Chemical and Energy Engineering, Universiti Teknologi Malaysia, 81310, Johor Bahru, Johor, Malaysia

ARTICLE INFO

Keywords:
Co-pyrolysis
Empty fruit bunch
High-density polyethylene
Rice husk ash
Kinetics
Thermodynamics

ABSTRACT

Rice husk ash (RHA) has been used as a catalyst precursor but there are lack of studies on the application of the resulting catalyst. This study allows researchers to have an insight on using RHA-sourced catalysts in pyrolysis and be encouraged to utilize waste materials in the future. The goal of this study is to examine the effect of catalysts derived from rice husk ash (RHA) using the solvent-free method, labelled as RHA-T, on the catalytic co-pyrolysis of empty fruit bunch (EFB) and high-density polyethylene (HDPE) via thermogravimetric analyser (TGA). Comparisons were then made with co-pyrolysis and catalytic co-pyrolysis over raw RHA and Hydrogen-exchanged Zeolite Socony Mobil-5 (HZSM-5). Thermogravimetric analysis was conducted (EFB-to-HDPE mass ratio of 1:1, catalyst-to-feedstock mass ratio of 1:1) in a nitrogen atmosphere, where samples were heated from 30 °C until 700 °C (heating rate 20 °C/min). The order of runs with highest mass loss in the second phase is as follows, with the term 'BP' indicating the biomass-plastic feedstock: BP-RHA-T (98.17 wt%), BP-RHA (96.25 wt %), BP (86.82 wt%) and BP-HZSM-5 (70.59 wt%). Kinetic analysis using Coats-Redfern method and comparing between different diffusional reaction models showed that using BP-RHA-T follows a one-dimensional diffusion reaction, similar to the non-catalytic run. Using RHA-T resulted in higher activation energy (83.03 kJ/mol to 84.91 kJ/mol) compared to the non-catalytic run (62.39 kJ/mol to 68.97 kJ/mol). Thermodynamic analysis showed the pyrolysis runs were endothermic and non-spontaneous. Using RHA-T resulted in a higher change of enthalpy, a lower change of Gibbs free energy and a less negative change of entropy. It can be concluded that applying catalysts synthesized using low-cost materials like RHA can improve the degradation of EFB and HDPE via pyrolysis, compared to commercial HZSM-5 catalysts.

1. Introduction

The challenges with fossil fuels have led to the increase in exploration of renewables, including biomass as a source of energy. Despite fossil fuels having high energy density and cheap availability, its extensive usage as transportation fuel has led to several consequences. Fossil fuels have been reported to be limited, implying that it will run out in the future (British Petroleum, 2020). Apart from that, fossil fuel is a major contributor of greenhouse gases (GHGs) emissions, especially carbon dioxide, around the world (Hannah Ritchie, 2017). Biomass, especially agricultural residues, is a low-cost renewable resource that is widely available and has the potential to be an alternative to fossil fuels.

In the Southeast Asian region, one of the top agricultural industries is the palm oil industry and around 30% of the recovered agricultural waste consists of empty fruit bunch (EFB) (Hosseini and Wahid, 2014). To convert biomass into valuable compounds, pyrolysis process is used to thermally degrade biomass at temperature range of 300–700 °C under inert atmosphere (Bhoi et al., 2020). From pyrolysis, biomass undergoes thermochemical conversion and produces bio-oil from condensed vapours, char and gas. Bio-oil is often desired due to its potential to be an

* Corresponding author.
E-mail address: vekes@utm.my (V. Balasundram).

https://doi.org/10.1016/j.clet.2022.100538
Received 30 April 2022; Received in revised form 6 July 2022; Accepted 14 July 2022
Available online 19 July 2022

alternative to transportation fuel, boiler fuel and can act as a gasoline enhancer (Kim et al., 2017). Depending on the lignocellulosic composition of the biomass, the bio-oil contains various chemical components including alcohols, ketones, acids, aldehydes and hydrocarbons (Chang, 2018). This is obtained from the degradation and further chemical reactions, such as depolymerization, decarbonylation, ring opening and closing and fragmentation, of the cellulose, hemicellulose, lignin components and their intermediates (Ansari et al., 2019). However, bio-oil derived from biomass is often obtained in low yield and mostly contains oxygenated compounds, making it unsuitable for commercial use, due to its low heating value of around 20 MJ/kg compared to commercial fuel (45.2 MJ/kg for diesel and 47.7 MJ/kg for gasoline) (Hossain et al., 2019). Thus, ongoing research including this study focuses on improving the qualities for bio-oil derived from biomass.

A way to improve bio-oil yield and quality is by introducing plastic to the biomass feedstock. Plastic has a relatively high hydrogen content compared to oxygen content and this assists the decomposition of biomass (Uzoejinwa et al., 2018). For example, Hassan et al. (2020) conducted a study on the addition of waste high-density polyethylene (HDPE) to sugarcane bagasse and found an increment in bio-oil yield (41.0–63.2 wt%) and also the hydrocarbon content (8.4–37.9 wt%) (Hassan et al., 2020). HDPE is one of the most common plastic types used and found as waste in countries such as Malaysia (World Wildlife Fund, 2020). Thus, utilizing plastic waste is not only beneficial for energy recovery but it can also redirect waste from the landfills.

Another way to improve bio-oil quality is with the addition of catalysts to the pyrolysis process. Since biomass-derived bio-oil contains a lot of oxygenated compounds, catalysts lower the oxygen content by promoting deoxygenation reactions, such as decarboxylation and decarbonylation of the pyrolysis vapours (Ro et al., 2018). Hydrogen-exchanged Zeolite Socony Mobil-5 (HZSM-5) has often been reported as an optimal catalyst for pyrolysis due its strong acidity and unique pore size (Muneer et al., 2019). HZSM-5 synthesis requires an alumina source, an organic template and an alkali component. However, the conventional materials used for the synthesis such as tetraethylorthosilicate (TEOS), can be dangerous when exposed to (Adam et al., 2012). Thus, studies are focusing on finding alternatives for a safer, low-cost materials for catalyst synthesis.

In conjunction with the utilization of waste for clean energy, rice husks, which is a form of waste from the rice industry, has attracted researchers due to its high silica content of approximately 96.2 wt% when converted to rice husk ash (RHA). This high silica content, makes this green material suitable to be used as a silica source for catalyst synthesis (Moayedi et al., 2019). There have been several studies that explored the methods of HZSM-5 synthesis using RHA as the silica source such as the solvent-free method, conducted by Zhang et al. (2019), and an organic template-free method, conducted by Dey et al. (2013). However, the application of the synthesized catalyst using RHA has not been extensively explored, especially in the application of pyrolysis. Other wastes like chicken eggshells and natural limestone from industry have been applied as catalysts to the pyrolysis process which shows the appeal of utilizing these materials in pyrolysis (Gan et al., 2018).

In addition, kinetic analysis is important to understand the behaviour of the pyrolysis process. The kinetic parameters include the activation energy (E_a) and the pre-exponential factor (A). Thermodynamic analysis also helps in the potential large-scale application of pyrolysis by determining parameters such as the change of enthalpy, ΔH, the change of Gibbs free energy, ΔG, and the change of entropy, ΔS. Thermogravimetric analysis (TGA) allows the observation of how material degrades in a controlled environment for pyrolysis and the data from TGA can be used to determine the kinetic and thermodynamic parameters.

This study applied the solvent-free synthesis method HZSM-5 catalyst using local RHA and used the synthesized catalyst for the catalytic co-pyrolysis of EFB and HDPE via TGA. These catalysts were compared with the co-pyrolysis and catalytic co-pyrolysis runs over raw RHA and HZSM-5 catalysts respectively. In addition, the results from TGA were used to conduct kinetic and thermodynamic analyses to further understand the reaction mechanism of the co-pyrolysis process.

2. Materials and methods

2.1. Feedstock preparation

Empty fruit bunch (EFB) and recycled high-density polyethylene (HDPE) was used as biomass and plastic waste feedstock respectively. The preparation of each feedstock was reported in our previous work (Shahdan et al., 2021), where the EFB and HDPE samples were prepared at a particle size of 0.5 mm.

2.2. Catalyst preparation and characterization

Rice husks were obtained from a local market in Malaysia. The preparation of rice husk ash was reported in our previous work (Shahdan et al., 2021) and labelled as 'RHA' for the purpose of this study.

In this study, RHA catalyst was synthesized using the solvent-free method applied from Zhang et al. (2019). This was done firstly mixing RHA, sodium aluminate, tetrapropylammonium bromide (TPABr) and sodium carbonate decahydrate in a beaker with a molar composition of 30 SiO_2: Al_2O_3:3.75 TPABr:9 $Na_2CO_3{\cdot}10H_2O$. The preparation method was applied following a previous study, with the final calcination modified to 750 °C for 4 h with a heating rate of 5 °C/min. The synthesized catalyst was labelled as 'RHA-T'. As a benchmark, HZSM-5 catalyst was also prepared. Commercial ZSM-5 in ammonium form was purchased from Alfa Aesar and calcined at 750 °C for 4 h at 5 °C/min to obtain HZSM-5.

For catalyst characterization, X-ray diffraction (XRD) was used to analyse the phase of the synthesized catalysts (PANalytical Empyrean X-ray diffractometer, United Kingdom). CuKα1 radiation with a wavelength (λ) of 0.15405 nm was used to irradiate the catalyst samples at a tube voltage of 40 kV and tube current of 30 mA. The sample scanning was carried out over a 2θ range from 3° to 60° with a scanning rate of 5 °C/min. Field emission scanning electron microscopy (FESEM) analysis (JEOL JSM-7800 F PRIME, Japan) was used to characterize the surface morphology of the synthesized catalysts. The catalyst sample was placed on the carbon stub and coated with platinum/palladium (Pt/Pd). An accelerating voltage of 5 kV was set in a vacuum condition. The magnification of FESEM image of catalysts was set to 10,000. Catalyst characterization for the Brunauer Emmett Teller (BET) specific surface area and porosity texture was also conducted. This was determined by nitrogen (N_2) physisorption at − 196 °C using an automatic gas adsorption analyser (ThermoScientific, Waltham, MA, USA). Fourier transform infrared spectroscopy (FTIR, Shimadzu IRTracer-100, Japan) analysis was conducted to characterize the vibration bands of the four catalysts. The spectra were collected between the range of 400–4000 cm^{-1} with a resolution of 4 cm^{-1}.

2.3. Experimental setup

The thermal degradation behaviour of empty fruit bunch (EFB) and high-density polyethylene (HDPE) feedstock over co-pyrolysis and catalytic co-pyrolysis conditions using HZSM-5, RHA, and RHA-T catalysts were performed via thermogravimetric analyser (TGA/SDTA851, METTLER TOLEDO, USA). Around 5 mg of samples were prepared with the EFB-to-HDPE ratio set to 1:1 and for the catalytic samples, the catalyst-to-feedstock ratio set to 1:1. The feedstock and catalyst was mixed together using a mortar and pestle for 5 min to ensure uniform mixing. Nitrogen was used to create an inert atmosphere for the pyrolysis runs with a flow rate of 150 mL/min. The samples were heated from 30 °C at a heating rate of 20 °C/min until 700 °C. The pyrolysis runs conducted were co-pyrolysis of EFB and HDPE, labelled as 'BP', and catalytic runs over the three catalysts respectively, labelled as 'BP-

HZSM-5', 'BP-RHA', and 'BP-RHA-T'. Thermogravimetric (TG) and derivative thermogravimetric (DTG) curves were collected from the TGA to observe the degradation pattern of the feedstock with and without the presence of the catalysts and used for kinetic and thermodynamic analysis.

2.4. Kinetic analysis

The kinetic parameters of the pyrolysis processes, the activation energy, E_a, and the pre-exponential factor, A, were determined using the Coats-Redfern (CR) method. The derivation of the CR method can be referred to in our previous work (Balasundram et al., 2017). Three reaction models that have been referred to in literature regarding solid state reactions were applied for the pyrolysis processes as shown below in Eqns. (1)–(3), labelled as 'Model 1', 'Model 2' and 'Model 3' respectively (Yu et al., 2013),

$$g_1(\alpha) = \alpha^2 \tag{1}$$

$$g_2(\alpha) = \alpha + (1-\alpha)\ln(1-\alpha) \tag{2}$$

$$g_3(\alpha) = \left(1 - \frac{2}{3}\alpha\right) - (1-\alpha)^{2/3} \tag{3}$$

where α is the fractional conversion of the sample, and $g(\alpha)$ is the reaction model. Model 1 is the one-dimensional diffusion of reactants; Model 2 is related to two-dimensional diffusion of reactants and Model 3 is related to three-dimensional diffusion reaction (Zhang et al., 2020). Eqns. (1)–(3) was applied to the linearized CR expression show below,

$$\ln\left[\frac{g_n(\alpha)}{T^2}\right] = \ln\left[\frac{AR}{\beta E_a}\left(1 - \frac{2RT}{E_a}\right)\right] - \frac{E_a}{RT} \tag{4}$$

where n is the reaction model number (1, 2 or 3), T is the temperature in Kelvin, R is the universal gas constant (8.3144 J/mol·K), and β is the heating rate (K/min). From the linearized expression of Eqn. (4), the data computed was used to generate an xy-plot to determine the values of E_a and A.

2.5. Thermodynamic analysis

For the determination of the thermodynamic parameters, the change of enthalpy, ΔH, the change of Gibbs free energy, ΔG, and the change of entropy, ΔS, the E_a and A was applied to the following equations,

$$\Delta H = E_A - RT \tag{5}$$

$$\Delta G = E_A + RT\ln\left(\frac{K_B T_m}{hA}\right) \tag{6}$$

$$\Delta S = \frac{\Delta H - \Delta G}{T_m} \tag{7}$$

where K_B is the Boltzman constant (1.381×10^{-23} J/K), h is Planck's constant (6.626×10^{-34} Js) and T_m is the temperature corresponding to the highest peak in the DTG curve (K) (Chen et al., 2021). Fig. 1 shows the research flow that was conducted for this study.

3. Results and discussion

3.1. Phase analysis

Fig. 2(a) and (b) shows the XRD pattern of raw rice husk ash (RHA) and HZSM-5 respectively as a benchmark for the synthesized catalysts. XRD pattern was plotted from 3° to 60° as no peaks were observed past 60°. In Fig. 2(a), the peaks seen are not intense and are broad indicating low crystallinity of the sample. In Fig. 2(b), the peaks seen in HZSM-5 are intense, indicating high crystallinity with characteristic peaks in the 2θ ranges of 7°–9°, 12°–16° and 23°–25°. Similar observations of the XRD pattern of HZSM-5 were also seen by Du et al. (2020), which confirms the structure of the HZSM-5 catalyst that was used for this

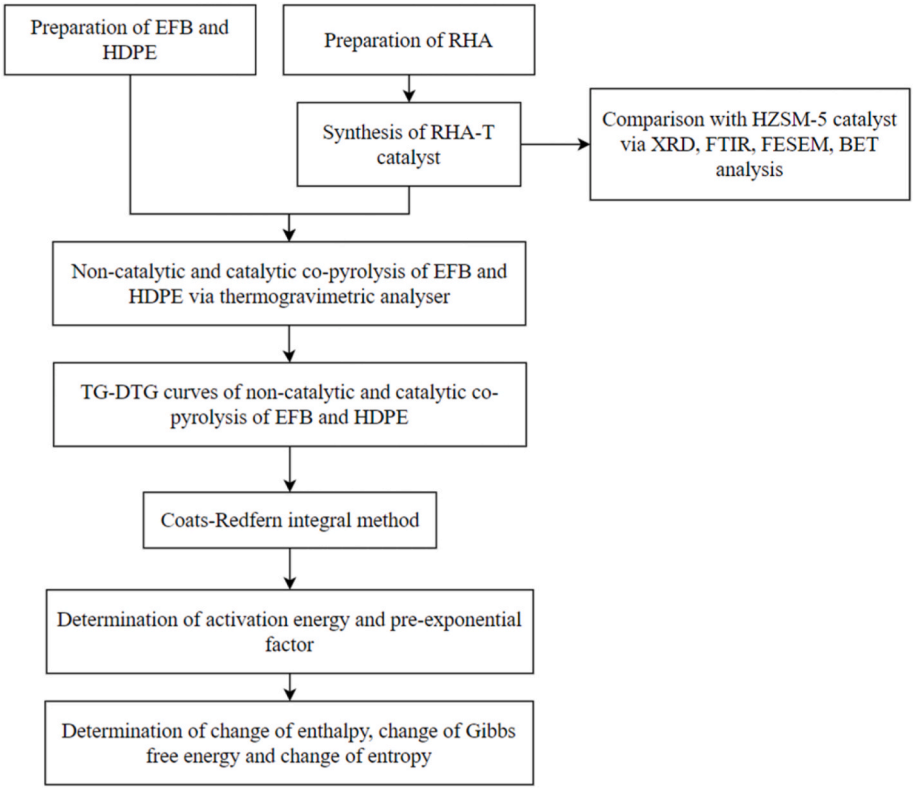

Fig. 1. Research flow for the thermogravimetric, kinetic and thermodynamic analysis of the co-pyrolysis of EFB and HDPE.

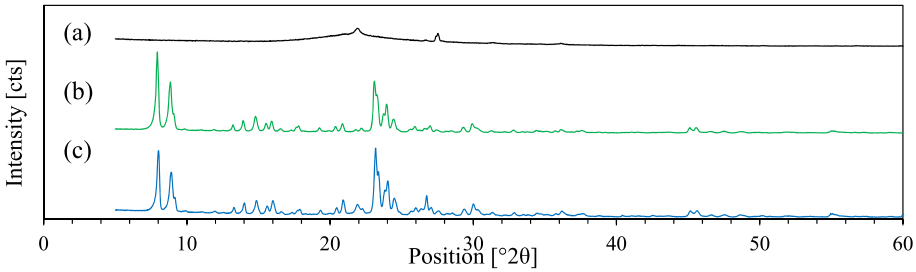

Fig. 2. XRD pattern for (a) raw RHA, (b) HZSM-5, and (c) RHA-T.

study. Fig. 2(c) of RHA-T, shows a similar XRD pattern to Fig. 2(b), indicating that the method of catalyst synthesis using RHA as a silica source, as conducted by Zhang et al. (2019), can be successfully repeated. Thus, it can be concluded that using RHA as green material rich in silica source and applying it in the solvent-free method for catalyst synthesis, a HZSM-5 structure can be obtained.

3.2. Surface morphology analysis

The surface morphology of raw RHA, HZSM-5, and RHA-T catalysts is shown in Fig. 3(a), 3(b), and 3(c) respectively. In Fig. 3(a), the raw RHA appeared to have a non-crystalline porous structure, with pores smaller than 1 μm. This low crystalline structure agrees with the XRD in Fig. 2(a). In Fig. 3(b), commercial HZSM-5 had irregular cubic-like structures which is homogenously distributed. The crystalline structure agrees with the XRD result in Fig. 2(b) where the intense peaks in the XRD pattern indicated high crystallinity. Widayat and Annisa (2017) also observed similar results where the high crystallinity of the HZSM-5 catalyst appeared to have distinct separated particles in the SEM analysis. Thus, this confirms the high crystallinity of the HZSM-5 catalyst. For RHA-T in Fig. 3(c), irregular rectangular shaped particles were seen on the catalyst sample. This implied that in addition to the HZSM-5 structure that was observed via XRD, the surface morphology of the RHA-T catalyst also appeared to be crystalline, and the irregular rectangular shaped particles observed was in an agreement to the results obtained by Zhang et al. (2019). This structure was managed to be achieved due to the presence of the organic template, TPABr, which helped to direct the silica from RHA and alumina from sodium aluminate into the HZSM-5 structure. Thus, the FESEM images confirmed the surface morphology of RHA-T is that of high crystallinity, similar to the HZSM-5 catalyst.

3.3. Framework vibration analysis

Fourier transform infrared spectroscopy (FTIR) was used to characterize the vibration bands of the catalysts as shown in Fig. 4. Fig. 4(a) until 4(c) shows the FTIR spectra for RHA, HZSM-5, and RHA-T respectively. It can be observed that all the FTIR spectra for the three catalysts shows strong absorption at around 1060 cm^{-1}, indicating the

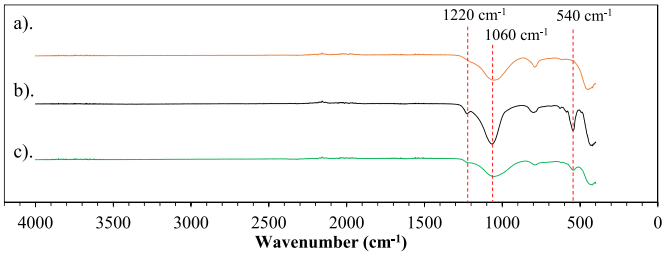

Fig. 4. FTIR spectra for (a) RHA, (b) HZSM-5 and (c) RHA-T.

vibration of the asymmetric Si–O–Si stretch, confirming the presence of silica in all the catalysts (Zhang et al., 2019). HZSM-5 catalyst contains a silica and alumina framework and thus, an Si–O–Si or Al–O–Al vibration band should be observed in the spectra. In Fig. 4(b), vibration bands were seen around 540 and 1220 cm^{-1} showing the presence of the characteristic double 5-rings of HZSM-5, which was previously reported by Dey et al. (2013). The spectrum of the raw RHA, on the other hand, does not show these vibration bands, as seen in Fig. 4(a). For RHA-T, the peaks around 540 and 1220 cm^{-1} can be observed (refer Fig. 4(c)), indicating that the double 5-rings of HZSM-5 were formed in RHA-T, although the absorption bands for RHA-T was not as intense as that for HZSM-5. The FTIR results align with the XRD and FESEM results and further confirmed the HZSM-5 structure that was obtained in the synthesized RHA-T catalyst.

3.4. Surface area and pore size analysis

Table 1 shows the textural and porosity properties of RHA, HZSM-5 and the synthesized RHA-T catalyst. Raw RHA was seen to have a small surface area with a large total pore volume and a large pore diameter. The large pores of the RHA are consistent with the FESEM results obtained where the pores are visible in Fig. 2(a). HZSM-5 was used as a benchmark to compare with RHA-T. After the synthesis of RHA-T, it was seen that the BET surface area increased from 4.0391 m^2/g to 205.16 m^2/g but it was not as large as the BET surface area of HZSM-5. This could be confirmed using the FESEM image in Fig. 2(c), where on

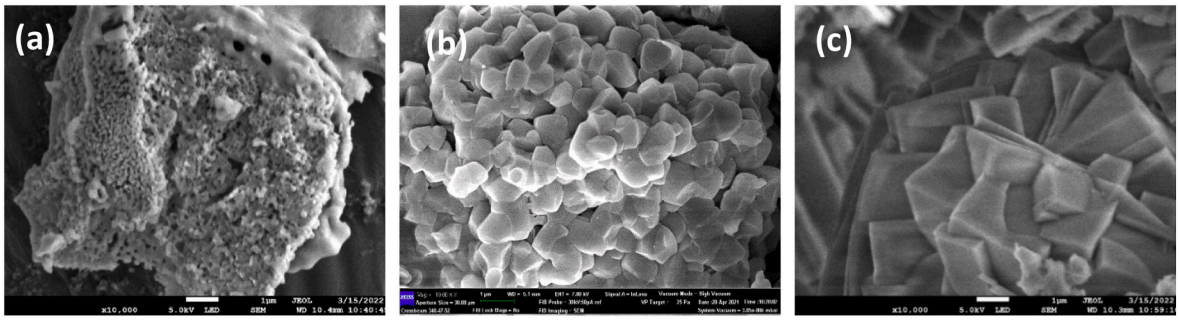

Fig. 3. FESEM images for (a) raw RHA, (b) HZSM-5 and (c) RHA-T.

Table 1
Textural properties for RHA, HZSM-5 and RHA-T.

Catalysts	BET Surface Area[a] (m^2/g)	Total Pore Volume[b] (cm^3/g)	Pore Diameter[c] (nm)
RHA	4.0391	0.2279	44.39
HZSM-5	365.81	0.0483	3.87
RHA-T	205.16	0.1206	4.06

[a] The BET surface area was obtained by the BET method.
[b] The total pore volume was determined from the absorbed amount of $P/P_0 = 0.99$.
[c] The pore diameter was obtained from the adsorption branches of the isotherms by the BJH method.

average, the particles of RHA-T appeared to be larger than that of HZSM-5 in Fig. 2(b). RHA-T also had larger total pore volume and pore diameter. As mentioned by Zhang et al. (2019), which also obtained similar results for catalysts synthesized using RHA, this could be due to the impurities that exist in RHA that could limit the formation of the catalyst framework as RHA does not contain 100% silica.

RHA contains approximately 96.2% silica, 1.62% potassium oxide, 0.36% magnesium oxide, and trace amounts of calcium oxide, sodium oxide, iron (III) oxide, aluminium oxide and phosphorus pentoxide (Moayedi et al., 2019). Since the characterization results thus far have shown that the synthesized RHA-T catalyst has a similar structure and textural properties to the HZSM-5 catalyst, it could be implied that the impurities in RHA does not significantly affect the final synthesized catalyst. However, to further confirm this, the synthesized catalyst should be applied in a chemical reaction to determine if the impurities would affect the catalytic activity, which is also explored in this study, in terms of the catalysing the degradation of the feedstock.

3.5. Co-pyrolysis of EFB and HDPE

3.5.1. Thermogravimetric analysis

Fig. 4 shows the TG curves of the co-pyrolysis and catalytic co-pyrolysis of EFB and HDPE over HZSM-5, RHA, and RHA-T. For TG analysis, catalyst mass was subtracted prior to calculations to clearly display the degradation pattern of the feedstock. As temperature progresses, hydrolysis, followed by fragmentation and depolymerization occurs on the feedstock and in Fig. 5, the degradation of EFB and HDPE was divided into three phases (Aysu and Durak, 2015). In phase I, slow mass loss was observed between room temperature and 200 °C, where moisture from the feedstock was removed. In phase II, rapid mass loss was observed between 200 °C and 540 °C, where lignocellulose from biomass and the HDPE polymer feedstock was degraded, fragmented and devolatilized. In phase III, degradation started to plateau between 540 °C and 700 °C. It can be seen in Fig. 4 that the degradation was significant in phase II due the degradation temperatures of EFB and HDPE being within the phase II range, where the lignocellulosic composition of EFB degrades anywhere around 240 °C–500 °C while HDPE starts to degrade around 430 °C (Wang et al., 2021). The presence of catalysts lowered the final degradation in phase II from 490 °C for all cases of the catalytic processes, with BP-RHA-T having the lowest final degradation temperature at 456 °C.

Fig. 6 shows the DTG curves of the co-pyrolysis and catalytic co-pyrolysis to further observe the rate of mass loss of the co-pyrolysis process and to determine the temperature where degradation is most rapid. The DTG curve was divided into the three different phases as mentioned previously. Three sets of peaks can be observed in Fig. 6, where the first set of peaks (between 30 °C and 120 °C) represent the mass loss of moisture, the second set of peaks (between 200 °C and 390 °C) represent the degradation of hemicellulose and cellulose in EFB, and the third set of peaks (between 390 °C and 520 °C) represent the degradation of HDPE polymer and lignin (EFB). It was seen that for all the runs, except for BP-HZSM-5, rate of mass loss is the highest within the 400 °C–500 °C range.

The percentage of volatilized matter (phase I, II, and III) and solid residual for the co-pyrolysis and catalytic co-pyrolysis samples is shown in Fig. 7. Overall, mass loss of volatilized matter is the highest in phase II for all the runs since degradation of EFB and HDPE occurs in phase II. The amount of volatilized matter for BP-HZSM-5 (70.59 wt%) in phase II was less than that of BP (86.82 wt%). This occurrence was also observed in a previous study of catalytic co-pyrolysis of polystyrene and sugarcane bagasse mixtures over HZSM-5 that generated lower bio-oil yield with higher yield of hydrocarbons in bio-oil (Iftikhar et al., 2019). Since TGA does not provide analysis on the composition of the volatilized matter, further research should be conducted on the composition of the volatilized matter to determine how catalysts affect the chemical composition of pyrolysis products. Using HZSM-5 did lead to increase in solid residual, as seen in Fig. 6, with 10.98 wt% compared to that of BP (4.31 wt%). This is related to the coking that occurred on the catalyst surface which is a drawback when using HZSM-5 catalysts (Kan et al., 2020).

For BP-RHA and BP-RHA-T, both of the runs have significantly higher amounts of mass loss in phase II, with the highest volatilized matter occurred BP-RHA-T at 98.17 wt%. In addition, it was seen that using RHA-T led to minimal solid residual (0.10 wt%). This could indicate that the catalytic activity of RHA-T is more effective in the degradation of EFB and HDPE than HZSM-5 and coking is less occurring on the catalyst.

From the TG results, overall, it appeared that using RHA-T in the co-pyrolysis run can increase the amount of volatilized matter with less solid residual produced compared to conventional HZSM-5. Again, further analysis should be conducted to investigate how using catalysts with RHA as a silica source affect the chemical composition of the volatilized matter.

3.5.2. Activation energy and pre-exponential factor

The kinetic parameters of the co-pyrolysis and catalytic co-pyrolysis of EFB and HDPE over HZSM-5, RHA and RHA-T calculated from TGA data and the application of Coats-Redfern (CR) method is shown in Table 2. From the linear regression of the CR method, R^2 were obtained to observe how closely the pyrolysis reaction is related to the reaction models applied. From Table 2, the R^2 value for all of the runs were above 0.90. Thus, it can be concluded that the pyrolysis reaction closely follows the diffusional models. Specifically, BP and BP-RHA-T closely follow Model 1, while BP-HZSM-5 and BP-RHA closely follow Model 3, as indicated by the bolded rows in Table 3. The runs that closely follow

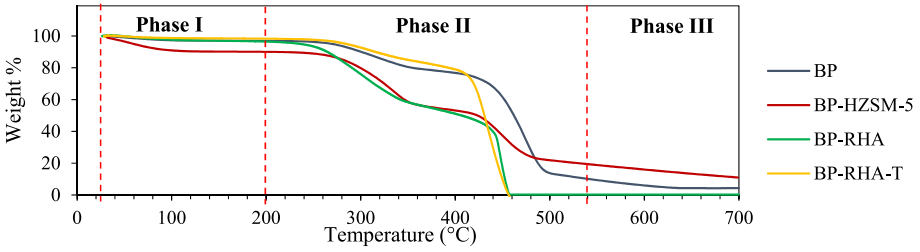

Fig. 5. TG curves of co-pyrolysis and catalytic co-pyrolysis of EFB and HDPE.

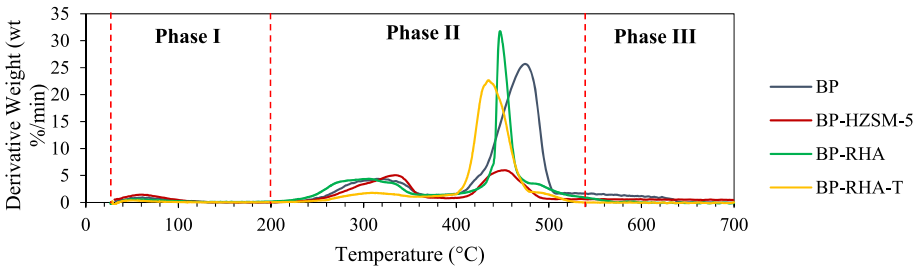

Fig. 6. DTG curves of co-pyrolysis and catalytic co-pyrolysis of EFB and HDPE.

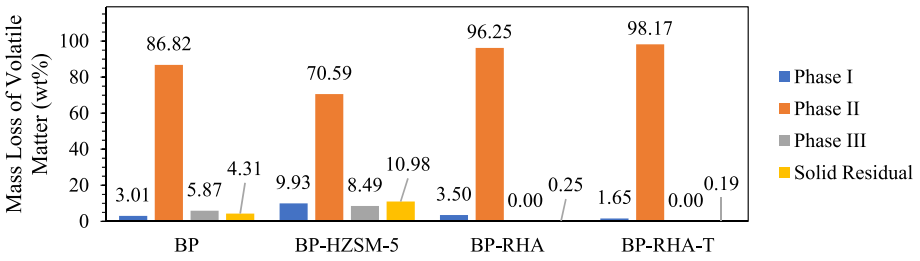

Fig. 7. TG volatile matter mass loss of EFB and HDPE feedstock.

Table 2
Kinetic parameters for co-pyrolysis and catalytic co-pyrolysis of EFB and HDPE.

Run	Model	E (kJ/mol)	A (min^{-1})	R^2
BP	**1**	**62.39**	**2064.51**	**0.964**
	2	67.02	3130.08	0.955
	3	68.97	1103.36	0.951
BP-HZSM-5	1	38.06	47.56	0.948
	2	43.00	86.16	0.958
	3	**45.06**	**32.45**	**0.961**
BP-RHA	1	58.62	2797.11	0.932
	2	68.57	15223.35	0.936
	3	**70.04**	**4890.98**	**0.938**
BP-RHA-T	**1**	**84.91**	**9.66×10^7**	**0.954**
	2	83.03	5.84×10^4	0.937
	3	84.33	1.77×10^4	0.931

Table 3
Thermodynamic parameters for co-pyrolysis and catalytic co-pyrolysis of EFB and HDPE.

Run	Model	ΔH (kJ/mol)	ΔG (kJ/mol)	ΔS (kJ/mol·K)
BP	**1**	**56.18**	**203.65**	**−0.20**
	2	60.81	205.70	−0.19
	3	62.76	214.12	−0.20
BP-HZSM-5	1	32.04	197.75	−0.23
	2	36.97	199.10	−0.22
	3	**39.03**	**207.05**	**−0.23**
BP-RHA	1	52.63	192.79	−0.19
	2	62.58	192.60	−0.18
	3	**64.05**	**200.87**	**−0.19**
BP-RHA-T	**1**	**79.02**	**155.17**	**−0.11**
	2	77.14	196.92	−0.17
	3	78.45	205.24	−0.18

Model 1 is most likely due to the flat structure of the particles resulting in one-dimensional diffusion since the EFB feedstock is fibrous, the HDPE feedstock was in the form of thin flakes and the RHA-T structure is flat as seen in Fig. 2(c). Meanwhile, BP-HZSM-5 and BP-RHA closely follows Model 3 due to the irregular cubic-like structure of HZSM-5 and the porous structure of RHA.

Regarding the kinetic parameters, the activation energy (E_a) is defined by the amount energy needed to break the bond for reaction to occur while the pre-exponential factor (A) indicates how fast the reaction rate is (Zhang et al., 2020). BP-HZSM-5 had an E_a range of 38.06–45.06 kJ/mol, which was lower than that for the co-pyrolysis, BP, indicating that the use of HZSM-5 lowers the energy barrier of the co-pyrolysis process. However, the A values for BP-HZSM-5 were significantly lower than that of BP, seen in Table 2, and this implies that although HZSM-5 can reduce the energy barrier, there is slower reaction rate of the pyrolysis vapour on the catalyst pores. This might also be the reason why there is an increase in solid residual when HZSM-5 is used, as seen in Fig. 6, because the slow reaction rate led to secondary reaction on the catalyst surface, further resulting in coking. For BP-RHA, the E_a values had a range between 58.62 and 70.04 kJ/mol which was neither higher nor lower that the E_a values for BP. However, the A values were higher than that of BP and BP-HZSM-5, indicating faster reaction rates, leading to more volatilized matter despite the values of the E_a. Finally, for BP-RHA-T, the E_a values were the largest, ranging from 83.03 to 84.91 kJ/mol but the A values were also the largest with four to seven times the order of magnitude (1.77×10^4 to 9.66×10^7 min^{-1}) compared to the other runs. This could imply that although the energy barrier when using RHA-T was high, the reaction rate was very fast and this allowed the energy barrier to be overcome, leading to the high amount of volatilized matter seen in Fig. 6.

From the kinetic analysis, the addition of HZSM-5 catalyst led to a decrease in activation energy compared to the non-catalytic run, while the addition of the RHA and RHA-T catalyst led to the increase of activation energy. However, the pre-exponential factors of BP-RHA and BP-RHA-T were significantly higher than that of BP-HZSM-5, which increased the degradation of the feedstock due to very rapid reaction rates.

3.5.3. Enthalpy, Gibbs energy and entropy

The thermodynamic parameters calculated using the activation energy, E_a, and the pre-exponential factor, A, is shown in Table 3, with bolded values indicating model in which the run is closely related to. The change of enthalpy, ΔH, represents heat absorbed, if positive, or heat released, if negative, during the reaction. In general, it was seen in Table 3 that all runs, both with and without catalysts had positive ΔH values. This implies that the pyrolysis process absorbs heat from the surrounding, which is also known as an endothermic process. Referring to the model which closely relates to the run, BP-RHA-T absorbed the most amount of heat (79.02 kJ/mol) while BP-HZSM-5 absorbed the least amount of heat (39.03 kJ/mol). This high amount of heat absorbed

allowed BP-RHA-T to have the most matter volatilized compared to BP-HZSM-5.

The change of Gibbs free energy, ΔG, indicates the spontaneity of a reaction, where the more negative the value, the more spontaneous the reaction is while the more positive the value, the more non-spontaneous the reaction is. In Table 3, all of the runs had a positive ΔG, implying that the pyrolysis reaction is non-spontaneous, since heat is applied to the reaction. Referring to the model which closely relates to the run, it can be seen that BP-RHA (200.87 kJ/mol) and BP-RHA-T (155.17) had smaller ΔG values compared to the non-catalytic run, suggesting that the presence of catalysts facilitates the pyrolysis reaction.

The change of entropy, ΔS, represents the degree of disorder in the system. The ΔS values for all the runs were found to be negative, indicating that the system becomes less disordered, due to reaching a thermal equilibrium (Majid et al., 2021). Comparing the ΔS for BP with the other runs, the presence of HZSM-5 decreased the ΔS to −0.23 kJ/mol·K, while the presence of RHA and RHA-T increased the ΔS to −0.19 kJ/mol·K and −0.11 kJ/mol·K respectively. The closer the ΔS value is to becoming positive, the more the system becomes more reactive and disordered, resulting in more volatilization of matter (Loy et al., 2019). The ΔS values agree with what was observed in the phase breakdown in Fig. 6, where BP-HZSM-5 produced less volatilized matter, compared to the other runs.

From the thermodynamic analysis, it was determined that the pyrolysis process is an endothermic, non-spontaneous process. The addition of catalysts, specifically the RHA-T catalysts, helped increase the reactivity of the system, according to the ΔH, ΔG and ΔS, by absorbing more heat into the system, enabling the volatilization of feedstock.

4. Conclusions

Rice husk ash (RHA) was used as a silica source for the synthesis of HZSM-5 catalyst, labelled as RHA-T, and compared with raw RHA and conventional HZSM-5. The co-pyrolysis and catalytic co-pyrolysis of empty fruit bunch (EFB) and high-density polyethylene (HDPE) over raw RHA, HZSM-5, and RHA-T was successfully conducted using a thermogravimetric analyser. Among the different catalysts, using RHA-T in co-pyrolysis led to the highest volatilization of matter in phase II (between 200 °C and 540 °C) of 98.17 wt% compared to using HZSM-5 (70.59 wt%).

From kinetic analysis, the co-pyrolysis process over RHA-T catalyst (BP-RHA-T) closely followed the one-dimensional diffusion reaction with a high activation energy of 84.91 kJ/mol. However, the pre-exponential factor for BP-RHA-T was significantly higher than that of other runs, allowing the energy barrier to be overcome. From the thermodynamic analysis, using RHA-T resulted in the most heat absorbed during the reaction (79.02 kJ/mol), which aligned with BP-RHA-T having the most volatilized matter. Using RHA-T lowered the change of Gibbs free energy of the reaction, increasing the spontaneity of the reaction and increased the change of entropy of the reaction, indicating higher reactivity for the co-pyrolysis process.

From this study, it can be seen that RHA, a silica-rich green material, is suitable to be used for catalyst synthesis and the synthesized catalyst can be applied in pyrolysis. From the determined kinetic and thermodynamic parameters, using RHA-based catalysts in the co-pyrolysis process was shown to increase the reactivity of the process, increasing the amount of volatilized matter. Thus, this encourages the utilization of waste as a low-cost energy feedstock and the utilization of green material for catalyst synthesis. Further analysis on the impact of using RHA-T catalysts on the chemical composition of the volatilized matter using gas chromatography-mass spectrometry (GC-MS) as well as determining the reaction mechanism are recommended.

Declaration of competing interest

The authors declare that they have no known competing financial interests or personal relationships that could have appeared to influence the work reported in this paper.

Acknowledgement

A special thanks to Universiti Teknologi Malaysia (UTM) for the financial support to carry out this research project under the Research University Grant - UTM ER (Vot number: Q. K130000.3843.19J46).

References

Adam, F., Appaturi, J.N., Iqbal, A., 2012. The utilization of rice husk silica as a catalyst: review and recent progress. Catal. Today 190, 2–14. https://doi.org/10.1016/j.cattod.2012.04.056.

Ansari, K.B., Arora, J.S., Chew, J.W., Dauenhauer, P.J., Mushrif, S.H., 2019. Fast pyrolysis of cellulose, hemicellulose, and lignin: effect of operating temperature on bio-oil yield and composition and insights into the intrinsic pyrolysis chemistry. Ind. Eng. Chem. Res. 58 (35), 15838–15852. https://doi.org/10.1021/acs.iecr.9b00920.

Aysu, T., Durak, H., 2015. Thermochemical conversion of Datura stramonium L. by supercritical liquefaction and pyrolysis processes. J. Supercrit. Fluids 102, 98–114. https://doi.org/10.1016/j.supflu.2015.04.008.

Balasundram, V., Ibrahim, N., Kasmani, R.M., Hamid, M.K.A., Isha, R., Hasbullah, H., Ali, R.R., 2017. Thermogravimetric catalytic pyrolysis and kinetic studies of coconut copra and rice husk for possible maximum production of pyrolysis oil. J. Clean. Prod. 167, 218–228. https://doi.org/10.1016/j.jclepro.2017.08.173.

Bhoi, P.R., Ouedraogo, A.S., Soloiu, V., Quirino, R., 2020. Recent advances on catalysts for improving hydrocarbon compounds in bio-oil of biomass catalytic pyrolysis. Renew. Sustain. Energy Rev. 121, 109676 https://doi.org/10.1016/j.rser.2019.109676.

British Petroleum, 2020. In: B (Ed.), Bp Statistical Review of World Energy 2020. London.

Chang, S.H., 2018. Bio-oil derived from palm empty fruit bunches: fast pyrolysis, liquefaction and future prospects. Biomass Bioenergy 119, 263–276. https://doi.org/10.1016/j.biombioe.2018.09.033.

Chen, F., Zhang, F., Yang, S., Liu, H., Wang, H., Hu, J., 2021. Investigation of pyrolysis kinetics, thermodynamics, product characteristics and reaction mechanism of rubber seed oil. Energy Convers. Manag., 244114535 https://doi.org/10.1016/j.enconman.2021.114535.

Dey, K.P., Ghosh, S., Naskar, M.K., 2013. Organic template-free synthesis of ZSM-5 zeolite particles using rice husk ash as silica source. Ceram. Int. 39, 2153–2157. https://doi.org/10.1016/j.ceramint.2012.07.083.

Du, H., Zhong, Z., Zhang, B., Shi, K., Li, Z., 2020. Comparative study on pyrolysis of bamboo in microwave pyrolysis-reforming reaction by binary compound impregnation and chemical liquid deposition modified HZSM-5. J. Environ. Sci. 94, 186–196. https://doi.org/10.1016/j.jes.2020.03.014.

Gan, D.K.W., Loy, A.C.M., Chin, B.L.F., Yusup, S., Unrean, P., Rianawati, E., Acda, M.N., 2018. Kinetics and thermodynamic analysis in one-pot pyrolysis of rice hull using renewable calcium oxide based catalysts. Bioresour. Technol. 265, 180–190. https://doi.org/10.1016/j.biortech.2018.06.003.

Hassan, H., Hameed, B.H., Lim, J.K., 2020. Co-pyrolysis of sugarcane bagasse and waste high-density polyethylene: synergistic effect and product distributions. Energy 191, 116545. https://doi.org/10.1016/j.energy.2019.116545.

Hossain, M.S., Ferdous, J., Islam, M.S., Islam, M.R., Mustafi, N.N., Haniu, H., 2019. Production of liquid fuel from co-pyrolysis of polythene waste and rice straw. Energy Proc. 160, 116–122. https://doi.org/10.1016/j.egypro.2019.02.126.

Hosseini, S.E., Wahid, M.A., 2014. Utilization of palm solid residue as a source of renewable and sustainable energy in Malaysia. Renew. Sustain. Energy Rev. 40, 621–632. https://doi.org/10.1016/j.rser.2014.07.214.

Iftikhar, H., Zeeshan, M., Iqbal, S., Muneer, B., Razzaq, M., 2019. Co-pyrolysis of sugarcane bagasse and polystyrene with ex-situ catalytic bed of metal oxides/HZSM-5 with focus on liquid yield. Bioresour. Technol. 289, 121647 https://doi.org/10.1016/j.biortech.2019.121647.

Kan, T., Strezov, V., Evans, T., He, J., Kumar, R., Lu, Q., 2020. Catalytic pyrolysis of lignocellulosic biomass: a review of variations in process factors and system structure. Renew. Sustain. Energy Rev. 134, 110305 https://doi.org/10.1016/j.rser.2020.110305.

Kim, Y.-M., Jae, J., Kim, B.-S., Hong, Y., Jung, S.-C., Park, Y.-K., 2017. Catalytic co-pyrolysis of torrefied yellow poplar and high-density polyethylene using microporous HZSM-5 and mesoporous Al-MCM-41 catalysts. Energy Convers. Manag. 149, 966–973. https://doi.org/10.1016/j.enconman.2017.04.033.

Loy, A.C.M., Yusup, S., How, B.S., Yiin, C.L., Chin, B.L.F., Muhammad, M., Gwee, Y.L., 2019. Uncertainty estimation approach in catalytic fast pyrolysis of rice husk: thermal degradation, kinetic and thermodynamic parameters study. Bioresour. Technol. 294122089 https://doi.org/10.1016/j.biortech.2019.122089.

Majid, M., Chin, B.L.F., Jawad, Z.A., Chai, Y.H., Lam, M.K., Yusup, S., Cheah, K.W., 2021. Particle swarm optimization and global sensitivity analysis for catalytic co-pyrolysis of Chlorella vulgaris and plastic waste mixtures. Bioresour. Technol. 329, 124874 https://doi.org/10.1016/j.biortech.2021.124874.

Moayedi, H., Aghel, B., Abdullahi, M.a.M., Nguyen, H., Safuan a Rashid, A., 2019. Applications of rice husk ash as green and sustainable biomass. J. Clean. Prod. 237, 117851 https://doi.org/10.1016/j.jclepro.2019.117851.

Muneer, B., Zeeshan, M., Qaisar, S., Razzaq, M., Iftikhar, H., 2019. Influence of in-situ and ex-situ HZSM-5 catalyst on co-pyrolysis of corn stalk and polystyrene with a

focus on liquid yield and quality. J. Clean. Prod. 237117762 https://doi.org/10.1016/j.jclepro.2019.117762.
Ritchie, H., 2017. Fossil fuels. https://ourworldindata.org/fossil-fuels. (Accessed 11 December 2021).
Ro, D., Kim, Y.-M., Lee, I.-G., Jae, J., Jung, S.-C., Kim, S.C., Park, Y.-K., 2018. Bench scale catalytic fast pyrolysis of empty fruit bunches over low cost catalysts and HZSM-5 using a fixed bed reactor. J. Clean. Prod. 176298–176303. https://doi.org/10.1016/j.jclepro.2017.12.075.
Shahdan, N.A., Balasundram, V., Shameli, K., Ibrahim, N., Isha, R., Tamunaidu, P., Abdul Manan, Z., 2021. Catalytic Co-pyrolysis of empty fruit bunch and high-density polyethylene. Chem. Eng. Trans. 89 https://doi.org/10.3303/CET2189035.
Uzoejinwa, B.B., He, X., Wang, S., El-Fatah Abomohra, A., Hu, Y., Wang, Q., 2018. Co-pyrolysis of biomass and waste plastics as a thermochemical conversion technology for high-grade biofuel production: recent progress and future directions elsewhere worldwide. Energy Convers. Manag. 163, 468–492. https://doi.org/10.1016/j.enconman.2018.02.004.
Wang, Z., Burra, K.G., Lei, T., Gupta, A.K., 2021. Co-pyrolysis of waste plastic and solid biomass for synergistic production of biofuels and chemicals-A review. Prog. Energy Combust. Sci. 84100899. https://doi.org/10.1016/j.pecs.2020.100899.
Widayat, W., Annisa, A.N., 2017. Synthesis and characterization of ZSM-5 catalyst at different temperatures. IOP Conf. Ser. Mater. Sci. Eng. 214, 012032 https://doi.org/10.1088/1757-899x/214/1/012032.
Wildlife Fund, World, 2020. Study on EPR scheme Assessment for packaging waste in Malaysia. https://wwfmy.awsassets.panda.org/downloads/study_on_epr_scheme_for_ packaging_waste_in_malaysia_wwfmy2020.pdf. (Accessed 17 May 2022).
Yu, J., Zeng, X., Zhang, J., Zhong, M., Zhang, G., Wang, Y., Xu, G., 2013. Isothermal differential characteristics of gas–solid reaction in micro-fluidized bed reactor. Fuel 103, 29–36. https://doi.org/10.1016/j.fuel.2011.09.060.
Zhang, C., Li, S., Bao, S., 2019. Sustainable synthesis of ZSM-5 zeolite from rice husk ash without addition of solvents. Waste Biomass Valorizat. 10, 2825–2835. https://doi.org/10.1007/s12649-018-0356-0.
Zhang, S., Liang, Y., Qian, X., Hui, D., Sheng, K., 2020. Pyrolysis kinetics and mechanical properties of poly(lactic acid)/bamboo particle biocomposites: effect of particle size distribution. Nanotechnol. Rev. 9 (1), 524–533. https://doi.org/10.1515/ntrev-2020-0037.